Dangling Chain Elastomers as Repeatable Fibrillar Adhesives

Metin Sitti,*,† Brian Cusick,‡ Burak Aksak,† Alper Nese,‡ Hyung-il Lee,‡ Hongchen Dong,‡ Tomasz Kowalewski,‡ and Krzysztof Matyjaszewski‡

Departments of Mechanical Engineering and Chemistry, Carnegie Mellon University, Pittsburgh, Pennsylvania 15213

ABSTRACT This work reports on repeatable adhesive materials prepared by controlled grafting of dangling hetero chains from polymer elastomers. The dangling chain elastomer system was prepared by grafting poly(*n*-butyl acrylate) (PBA) chains from prefunctionalized polydimethylsiloxane (PDMS) elastomer networks using atom transfer radical polymerization. To study the effects of chain growth and network strain as they relate to network adhesion mechanics, various lengths of PBA chains with degree of polymerizations (DP) of 65, 281, 508, and 1200 were incorporated into the PDMS matrix. PBA chains with a DP value of 281 grafted from a flat PDMS substrate showed the highest (~3.5-fold) enhancement of nano- and macroscale adhesion relative to a flat raw (ungrafted and not prefunctionalized) PDMS substrate. Moreover, to study the effect of PBA dangling chains on adhesion in fibrillar elastomer structures inspired by gecko foot hairs, a dip-transfer fabrication method was used to graft PBA chains with a DP value of 296 from the tip endings of mushroom-shaped PDMS micropillars. A PBA chain covered micropillar array showed macroscale adhesion enhancement up to ~7 times relative to the flat ungrafted prefunctionalized PDMS control substrate, showing additional nonoptimized ~2-fold adhesion enhancement due to fibrillar structuring and mushroom-shaped tip ending. These dangling hetero chains on elastomer micro-/nanofibrillar structures may provide a novel fabrication platform for multilength scale, repeatable, and high-strength fibrillar adhesives inspired by gecko foot hairs.

KEYWORDS: repeatible adhesives • dangling chains • elastomers • gecko • atom transfer radical polymerization

INTRODUCTION

The amazing climbing ability of geckos has recently been of great interest to scientists. Geckos can attach reversibly to surfaces with adhesion strengths as high as 10 N/cm^2 using predominantly van der Waals forces (1, 2). This remarkable adhesiveness of gecko foot hairs is believed to be rooted in their hierarchical structure, comprised of β-keratin micro-/nanoscale hairs (3, 4) with saucer-shaped tip endings (5–7) and a soft backing (8), which can conform easily to a surface roughness. These hairs have recently inspired elastomeric (6, 9–14) and rigid (15–17) polymer micro-/nanofibers and carbon nanotube (18–21) based fibrillar adhesives. The macroscale adhesion of gecko foot hairs is strong, since their micro-/nanofibrillar structuring increases effective compliance, enables flaw insensitivity and equal load sharing, and increases resistance to crack propagation by trapping the fracture locally (22, 23). Elastic hairs also enhance adhesion by stretching, which keeps a larger number of fibers in contact during detachment (6, 9, 22).

The work described herein was built upon the design principle that an adhesive material could be made that takes advantage of the flexibility of an elastomer to conform to a surface and maximize contact area. Elastomers, however, have the disadvantage of detaching from a target once the network strain becomes too high. The described study was driven by the expectation that this detriment can be minimized by the incorporation of hetero dangling polymer chains (immiscible with the matrix polymer) into soft polydimethylsiloxane (PDMS) networks (Figure 1). The immiscible, highly extensible, mobile dangling chains within the network should remain in a coiled globule and, after making good contact with an adhesion target, fully extend as the target retracts, dissipating energy as in the Lake–Thomas effect (24). Since the dangling chains are chemically attached to a compliant network backing, the backing itself is expected to be pulled behind the dangling chains, increasing the amount of work necessary to separate the surfaces. Upon final separation from the target, the dangling chains should recoil, allowing for repeatable use. The Lake–Thomas effect implies that, by increasing the length of the dangling chains, the material will dissipate more energy and thus exhibit stronger adhesion. At some point, however, as shown in schematically in Figure 1c, the longer dangling chains will occupy a greater volume within a network, causing internal strain that diminishes the adhesive capability of the material and perhaps even leading to material failure. In addition to adhesion enhancement due to dangling chain and backing layer elastomer network stretching, molecular "hairs" were also grafted from the tip endings of elastomeric mushroom-shaped micropillars inspired by gecko foot hairs, leading to further adhesion enhancement.

Given the present limits of top-down fabrication techniques, the smallest sizes in gecko-inspired polymer structures fabricated to date did not extend far below the submicrometer region. In the present work, in order to fabricate

* To whom correspondence should be addressed. E-mail: sitti@cmu.edu.
Received for review June 23, 2009 and accepted September 10, 2009
† Department of Mechanical Engineering.
‡ Department of Chemistry.
DOI: 10.1021/am9004368

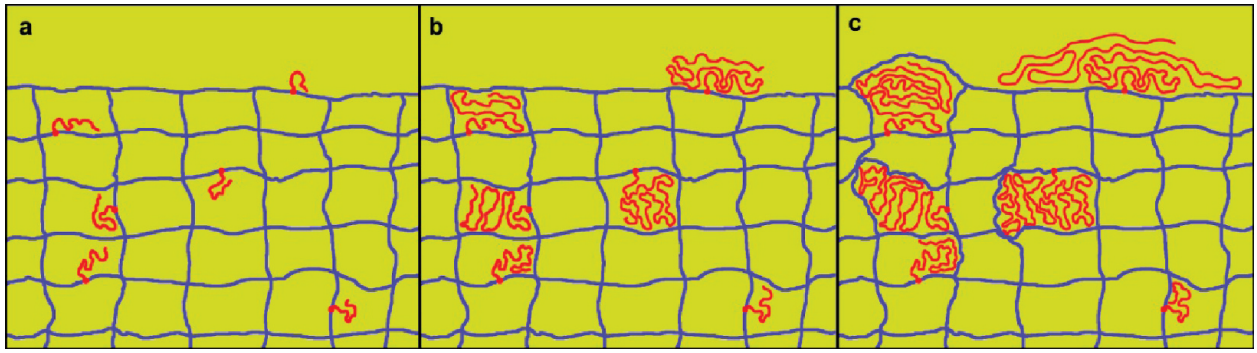

FIGURE 1. Cartoon representation of a dangling chain network. The PDMS (blue) forms the base of the network, while the PBA chains (red) compose the dangling chains for low-molecular-weight (a), medium-molecular-weight (b), and high-molecular-weight PBA (c).

the smallest scale repeatable fibrillar adhesive materials, we have resorted to the use of bottom-up, molecular level fabrication. This was made possible through the use of a controlled polymerization technique such as atom transfer radical polymerization (ATRP) (25) to "decorate" the surface and bulk of the compliant elastomeric backing material (PDMS) with poly(*n*-butyl acrylate) (PBA), which is highly extensible, mobile, and immiscible with PDMS (Figure 1) (26). Although ATRP-based polymerization is often used on rigid substrates, extending such a synthesis method to elastomeric substrates is less common (27). The uncontrolled incorporation of dangling chains into the PDMS network has been already shown to lower the Young modulus (28−31), an important factor in enhancing adhesion. The use of the ATRP technique in this study grants two levels of incorporation control: (1) control of the number of dangling chains through the concentration of ATRP initiator prebuilt into the PDMS network and (2) control of polymer chain length to maximize chain length, while minimizing network strain.

RESULTS AND DISCUSSION

To study the impact of dangling hetero chains on nano- and macroscale adhesion, we incorporated PBA chains into the bulk of PDMS. To show the effect of the backing layer compliance on chain adhesion, PBA chains were also grafted from silicon wafers. PDMS was selected as the elastomeric substrate material, since it is a well-characterized elastomer, which can be fabricated into fibrillar adhesive structures (10, 12−14). To study the dangling chain network adhesion mechanics, various lengths of PBA chains were grown from these substrates using both bulk and surface-initiated ATRP processes (27, 32, 33). As in all controlled polymerization processes, the length of the polymer chains was controlled by stopping the reaction at progressively increasing times. PBA chains with degrees of polymerization (DP) of 65, 281, 508, and 1200 were grafted from PDMS. Reference PBA chains on a rigid silicon substrate were prepared with DP values of 296 and 1050. The PBA film thicknesses measured by ellipsometry were 26 and 130 nm, corresponding to the grafting densities 0.41 and 0.55 chains/nm^2, respectively (Table 1). The degrees of polymerization were ascertained by gel permeation chromatography (GPC) analysis of a free polymer growing concurrently in solution. It should be noted

Table 1. Number Average Molecular Weight (M_n), Polydispersity Index (PDI = M_w/M_n), Degree of Polymerization (DP), Thickness, and Grafting Density Data of the Functionalized Materials

material	M_n(THF-GPC) (kDa)	PDI	DP (THF-GPC)	thickness (nm)	grafting density (chains/nm^2)
PDMS-*g*-PBA$_{65}$	8.5	1.24	65		
PDMS-*g*-PBA$_{281}$	36	1.09	281		
PDMS-*g*-PBA$_{508}$	65	1.07	508		
PDMS-*g*-PBA$_{1200}$	153	1.14	1200		
silicon-*g*-PBA$_{296}$	38	1.06	296	26	0.41
silicon-*g*-PBA$_{1050}$	134	1.08	1050	130	0.55

Table 2. SEM/EDX Composition Analysis[a]

material	amt of carbon (wt %)	amt of silicon (wt %)
raw PDMS	44.5 ± 1.3	33.4 ± 0.4
PDMS w/initiator	43.8 ± 0.9	33.4 ± 0.3
PDMS-*g*-PBA$_{281}$	51.3 ± 4.2	28.3 ± 3.5

[a] Average values over a whole cross section of the sample.

that whereas these numbers should accurately reflect the DP of chains grown from the surface (33), the DPs of chains grown within the bulk elastomer network may be considerably lower due to confinement effects. Indeed, the ATRP grafting of PBA into initiator-functionalized PDMS substrates resulted in a 21% increase in weight for the sample with a DP value of 281, clearly indicating that the dangling chains were incorporated throughout the bulk of the elastomer network, not only on the surface. Assuming full incorporation of the initiator into the network and 100% initiation efficiency, this mass increase would correspond to an average DP value of 47. This value is significantly lower than the DP value of 281 measured by GPC of chains grown in solution. Moreover, bulk incorporation was confirmed by scanning electron microscope energy dispersive X-ray (SEM-EDX) analysis of compositional profiles of exposed sections of the material, which showed the gradient of carbon enrichment and silicon depletion moving from the center of the cross sections toward the surface (Table 2). This indicates that the polymerization of PBA from the PDMS network, even in its swollen state, is still limited by diffusion of monomer into the PDMS network.

Tapping mode atomic force microscopy (AFM) images of raw PDMS and PDMS grafted with DP-281 PBA chains are

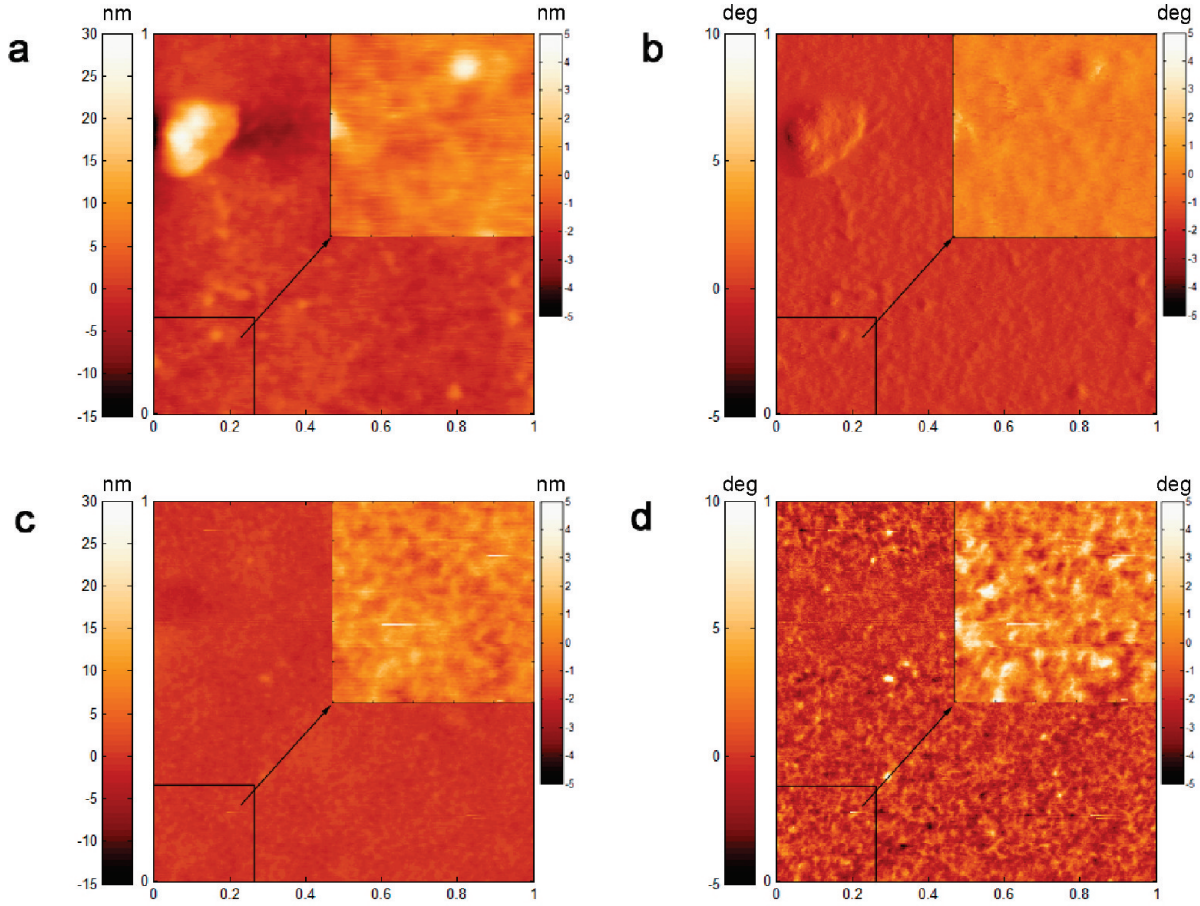

FIGURE 2. 1 × 1 μm atomic force microscope tapping mode images of raw PDMS and PBA-281 with 250 × 250 nm insets to show detail. The color scale for all insets is from −5 to +5 (nm or deg). (a) Height images of raw PDMS show a relatively flat and uniform surface, with a few large protrusions. (b) Phase images of raw PDMS show little material contrast. (c) Height images of PBA-281 show a more homogeneous surface, with small PBA domains. (d) Phase images show material contrast between the PBA domains/pockets and the PDMS.

shown in Figure 2. In height images, the surface of raw PDMS appeared to be relatively flat and uniform with occasional protrusions, ~100 nm across, possibly due to postsynthesis surface contamination of the material. On the sub 100 nm level, both height and phase images were relatively uniform and featureless, as expected for an unstructured, uniformly cross-linked elastomer. Height images of PDMS grafted with DP-281 PBA revealed the presence of nodular sub 25 nm domains, which appeared brighter (having less mechanical loss) than their surroundings in AFM phase images. Given the overall composition of the grafted material, these features were tentatively identified as domains of PBA chains.

Local nanoscale adhesion, or pull-off force, was studied using a contact mode AFM by measuring force−distance curves. Here, the deflection of the silicon AFM cantilever with a ~10 nm tip radius was continuously monitored, while the whole cantilever was repeatedly moved toward and away from the surface. Although some fibrillar nanoscale adhesion characterization studies were conducted in the past using flattened AFM probe tips (flat punch indenters) (13, 15), we chose to use imaging tips, which can be viewed as parabolic (and thus approximated near the tip as spherical), since they provide alignment error free measurements and represent a single asperity surface roughness, enabling one to characterize the rough surface adaptation and adhesion of the fibrillar structures (9). As a control, adhesion was also measured on flat silicon and PDMS substrates with and without the ATRP initiator, in an attempt to assess the pure contribution of dangling chains to adhesion.

To study the effect of the preload (the maximum normal force applied by the tip to the surface), the pull-off force (adhesion) was measured for preloads ranging from <10 to 350 nN at a probe retraction speed of 0.5 μm/s (Figure 1 in the Supporting Information). A total of 256 measurements were conducted at different locations in a 10 μm^2 area for each preload (Figure 3a). PBA chains with a DP value of 281 grafted from PDMS showed the highest nanoscale adhesion, especially for higher preloads. DP-508 chains gave slightly lower adhesion behavior, as did DP-1200 chains, except at high preloads. To show the effect of a compliant backing, adhesion measurements were also conducted on DP-296 and DP-1050 PBA chains grafted from silicon (Figure 2 in the Supporting Information). These samples showed preload-adhesion values similar to those of PDMS grafted with PBA DP-1200. It is evident from Figure 3a that longer chains provided up to 3−4 times higher adhesion values than either the short (DP-65) PBA chains or the flat control PDMS substrates with and without initiator. It is expected that the samples with longer PBA chains (DP-508 and DP-1200)

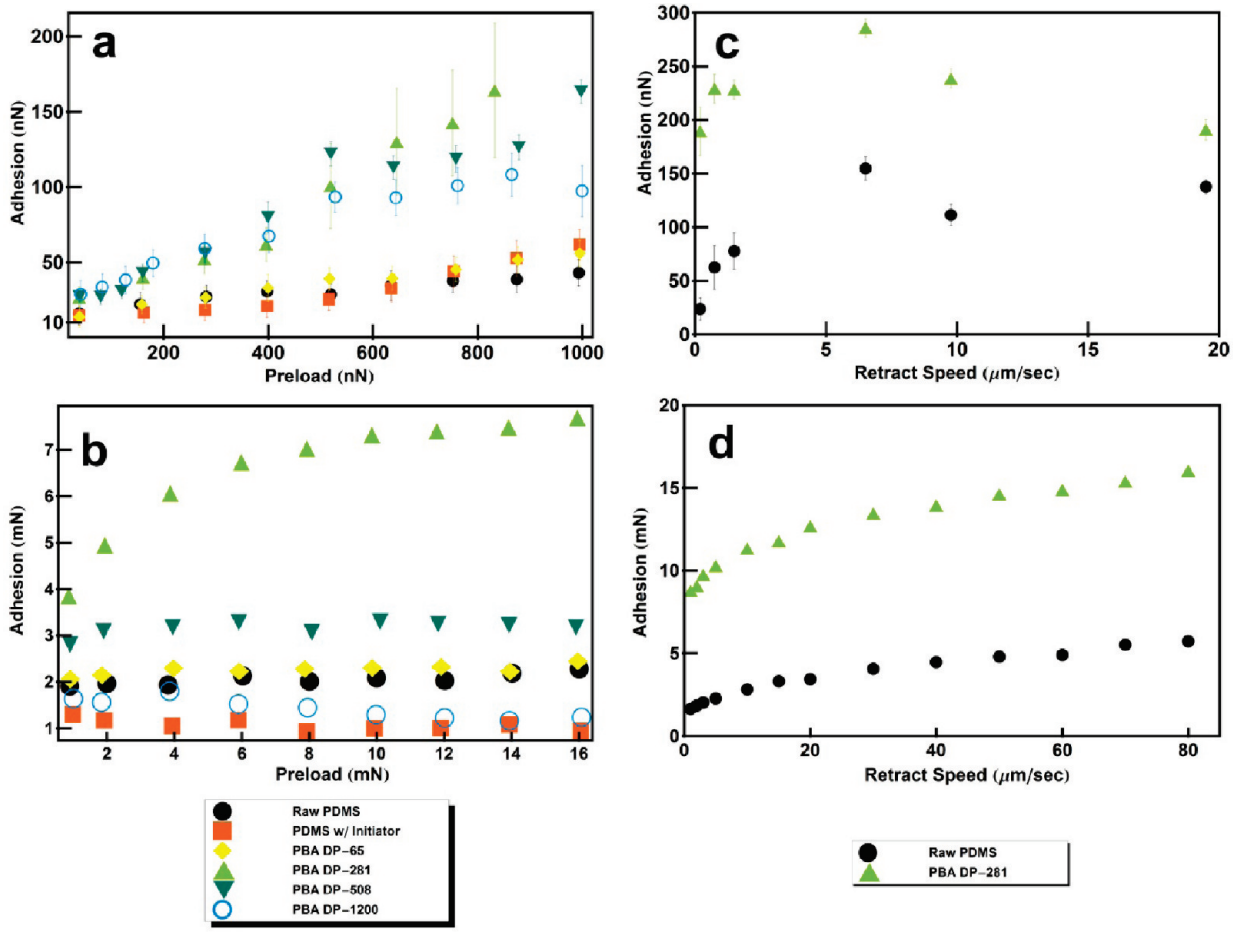

FIGURE 3. Experimental results of nano- and macroscale adhesion characterization of four different length PBA chains grafted from a PDMS substrate and two control flat PDMS substrates with and without the ATRP initiator: (a) nanoscale adhesion measurements carried out at a retraction speed of 0.5 μm/s using a silicon AFM probe tip with 10 nm radius; (b) macroscale adhesion measurements carried out at a retraction speed of 1 μm/s with a 6 mm diameter smooth glass hemisphere; (c) nanoscale and (d) macroscale adhesion results for different retraction speeds.

would show greater adhesion than the DP-281 sample, since stretching of longer chains should be associated with more energy dissipation. However, Figure 3a shows that adhesion actually decreases past DP-281. Further analysis of the apparent Young modulus (estimated from the indentation part of the force–distance curve) and of the pull-out length (the distances by which the sample had to be moved away from the probe for the probe deflection to go from its minimum to the zero on the retract portion of the force–distance curve) of the AFM probe reveal that samples with longer PBA samples are slightly stiffer and show shorter pull-out lengths. This suggests that incorporation of longer PBA chains prestretches the PDMS network, leading to the increased rigidity of the sample. Such stiffening of the PDMS network would prevent the network from being pulled behind the PBA chains. As described next, the pull-out of the compliant backing substrate appears to be the key prerequisite of enhanced adhesion.

The apparent Young modulus and pull-out length were correlated for both a low preload (Figure 4a, 50 nN) and a high preload (Figure 4b, 350 nN). At both preloads, sample PBA DP-281 showed both lower apparent Young modulus and higher pull-out lengths than the other samples. This additional information provided significant insight into the dependence of adhesion on the pull-out length and on the compliance of the PDMS substrate. Higher pull-out lengths are clearly associated with more energy dissipation, leading to higher adhesion, and a soft, compliant backing can increase this pull-out length beyond that of a fully extended chain. Consequently, increasing the length of PBA chains leads to an increase in adhesion, but only up to the point when the PBA dangling chains become so long that their presence in the bulk of PDMS causes its undesirable stiffening. High enough preloads and a sharp indenter also lead to a possibility that subsurface dangling chains can contribute to further increased adhesion.

Variable-speed measurements were carried out in an attempt to show any correlation between nanoscale adhesion and retraction speed (Figure 3c). In this case, the adhesion initially increased and then decreased after the approach and retraction speed reached a value of about 7.5 μm/s. For raw PDMS, the adhesion also slightly decreased after this point, but not nearly as much as for PBA DP-281. Most likely, this adhesion loss was due to the inability of the PBA surface layer to behave as a viscous, energy-dissipative medium at higher deformation rates. Moreover, experiments were performed on the PDMS substrate with DP-281 PBA chains to test the repeatability of their high adhesion.

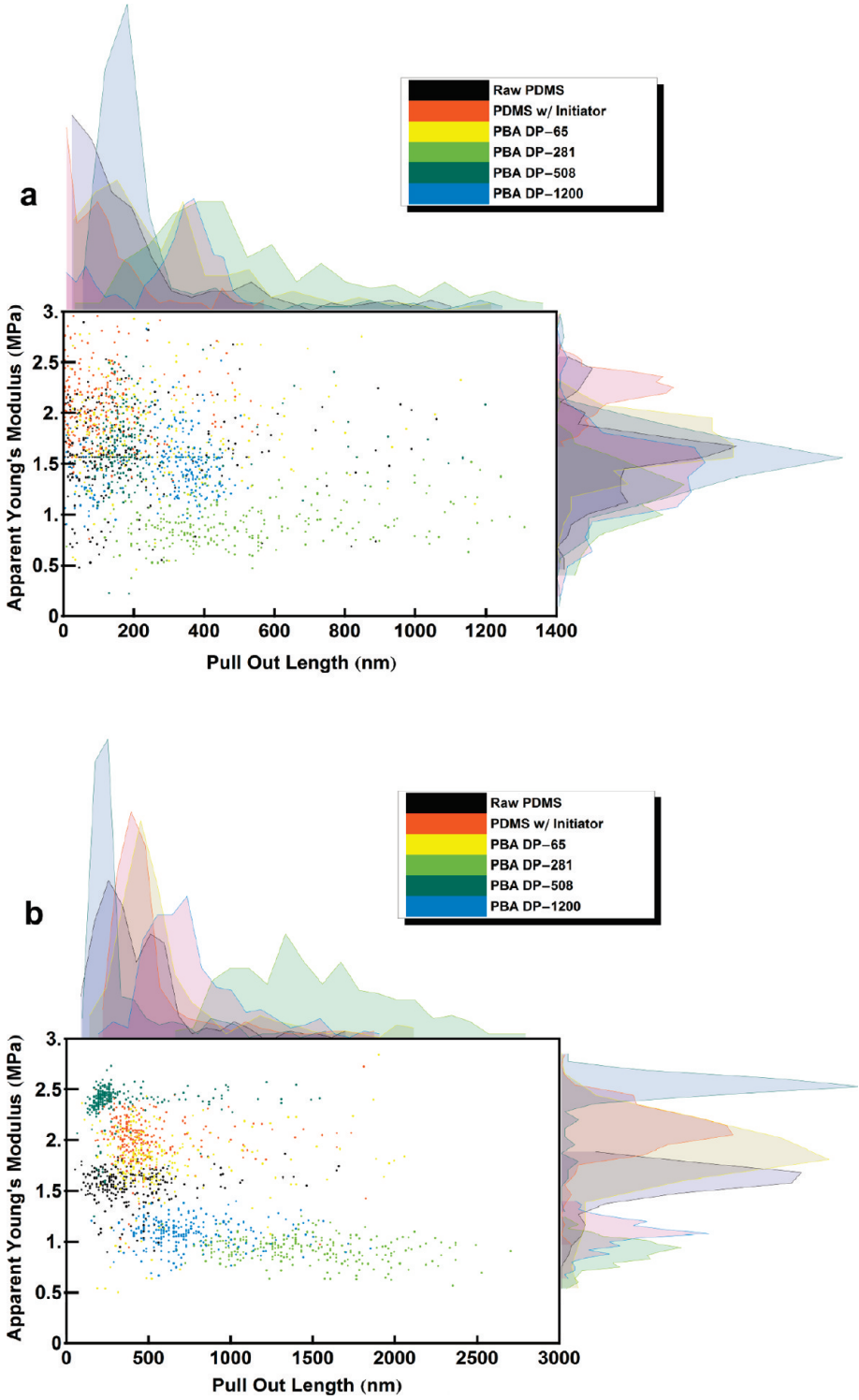

FIGURE 4. Correlation plots of the apparent Young moduli of the flat PDMS substrates with different DP values of PBA chains versus probe pull-out length at preloads of (a) 50 nN and (b) 350 nN. Corresponding distributions of apparent modulus and probe pull-out length are shown adjacent to the abscissa and coordinate axes.

After 256 adhesion measurements on the same spot at a high (350 nN) preload, the average value of pull-out force was equal to 54 ± 3 nN.

The macroscopic adhesion behavior of PBA chains on PDMS and silicon substrates was studied using an automated custom tensile adhesion characterization system (9) with an indenter comprised of a 6 mm diameter smooth glass hemisphere. Adhesion measurements were performed for preloads up to 16 mN (Figure 3b) at a retraction speed of 1 μm/s using force–distance curves (Figure 3 in the Supporting Information). For PBA chains on silicon substrates, there was no measurable adhesion, due to a very small macroscale contact area. For PBA chains on flat PDMS substrates, the results were very similar to those of the nanoscale measurements, where the PDMS substrate with DP-281 PBA chains showed significantly higher adhesion than the rest of the

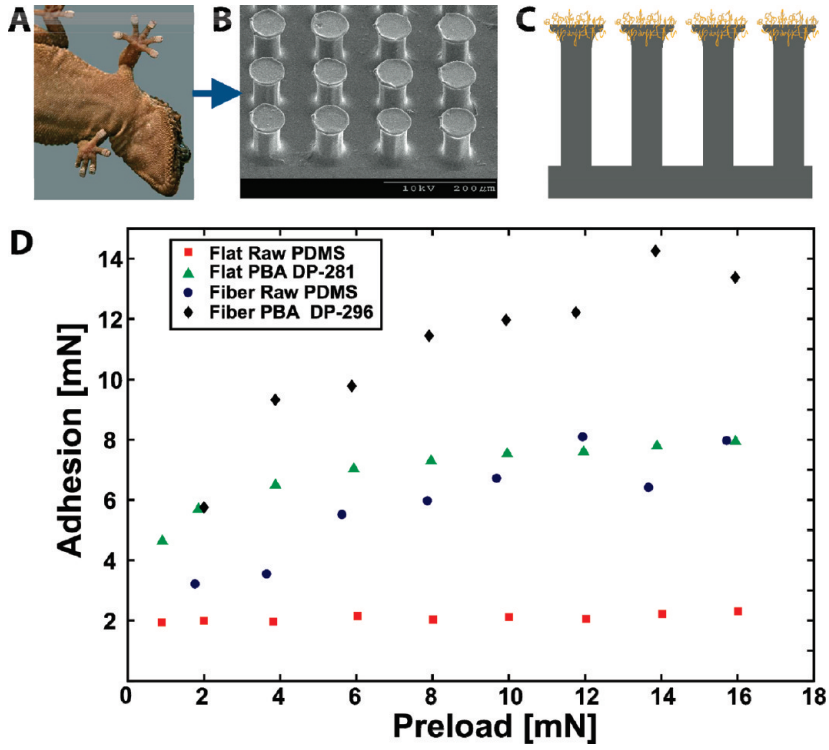

FIGURE 5. (A) Photograph of a *Bibron* gecko adhered to a glass surface. Scanning electron microscopy image (B) and schematic illustration of hierarchical geometry (C) of mushroom-shaped PDMS micropillars grafted with PBA chains on their tips. (D) Comparison of results of macroscale adhesion measurements carried out with bare and PBA-grafted flat PDMS substrates versus bare and PBA-grafted mushroom-shaped PDMS micropillar arrays (6 mm diameter glass hemisphere retracted at 1 μm/s).

samples. These chains had up to ~7 times higher adhesion than the PDMS control substrate with the ATRP initiator and up to ~3.5 times higher adhesion than the raw PDMS control substrate. Moreover, the speed effect on macroscale adhesion of PBA chains was measured (Figure 3d). These variable-speed measurements showed an increase in adhesion with an increase of retraction rate on the macroscale. Here, since the approach rate was held constant at 1 μm/s, the adhesion should be expected to change with the retraction rate only.

To study the effect of PBA chains on adhesion when they are grafted from fibrillar elastomer structures inspired by gecko foot hairs, the PBA chains were also incorporated into the tip endings of mushroom -shaped PDMS micropillars. In these experiments, we used 10 × 15 mm^2 PDMS micropillar arrays with a tip diameter of 86 μm, a length of 106 μm, a base diameter of 52 μm, a backing layer thickness of 1.2 mm, and a center-to-center spacing of 125 μm (see Figure 5a,b). Since PBA DP-281 chains gave the highest macro- and nanoscale adhesion enhancement results, similar DP PBA molecular chains with a DP value of 296 were grafted from the tip endings of mushroom-shaped pillars.

Adhesion measurements on these pillar arrays (Figure 5c) were carried out using the custom macroscale adhesion setup. The retraction and approach speeds were kept constant at 1 μm/s to minimize bulk viscoelastic effects with the preload ranging from 2 mN to 16 mN. A micropillar array with grafted PBA DP-296 chains exhibited the highest adhesion at all preloads in comparison to bare PDMS micropillars with the same geometry, flat raw PDMS, and flat PDMS with PBA DP-281 chains (Figure 5d). The adhesion of the PBA chain grafted micropillar array was up to ~7 times higher than the flat ungrafted PDMS control substrate adhesion and ~2 times higher than the flat PDMS with PBA DP-281 chains or ungrafted PDMS mushroom-shaped micropillars. The macroscale adhesion repeatability of grafted PDMS micropillars and grafted PDMS flat surfaces was characterized by measuring the adhesion of the hemispherical indenter at the same spot for 1000 times with a preload of 10 mN at 10 μm/s speed (Figure 6). After hundreds of cycles, the grafted pillar array pull-off force fluctuated about the initial pull-off value but in overall exhibited a steady value, which suggests a repeatable adhesive performance.

Altogether, nonoptimized micropillar structures enhanced adhesion over flat samples for both neat and PBA-grafted PDMS. Most importantly, the maximum adhesion enhancement was achieved by *combining* the nanoscale adhesion enhancement due to the presence of PBA dangling chains with the enhancement provided by the presence of elastomeric mushroom-shaped micropillars inspired by gecko foot hairs (6, 8).

In order to better understand the adhesion enhancement mechanism on the macroscale, the Young modulus and the thermodynamic work of adhesion of the raw PDMS and PBA DP-281 sample were characterized as explained in detail in Experimental Section. The measurements resulted in E = 2.39 MPa and w = 21.9 mJ/m^2 for raw PDMS and E = 1.51 MPa and w = 25.6 mJ/m^2 for PBA DP-281. The experimental results for pull-off forces at the macroscale showed up to about 3.5-fold adhesion enhancement for the PBA DP-281

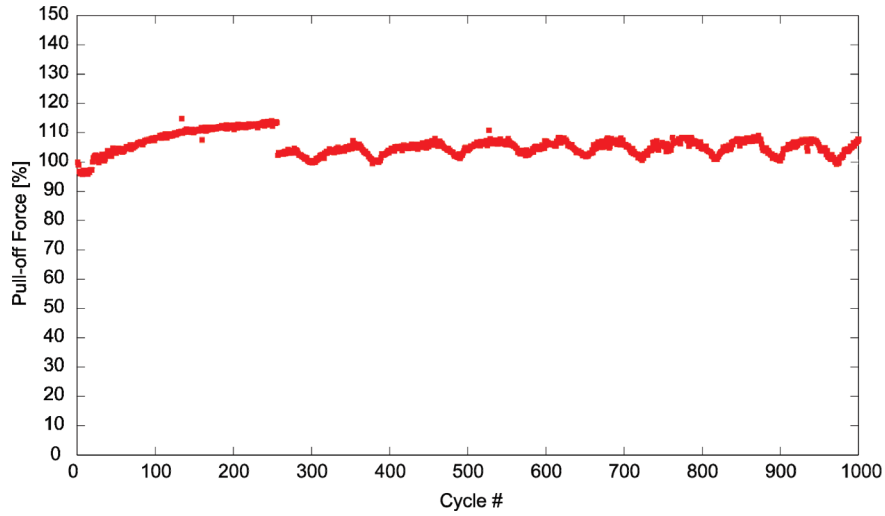

FIGURE 6. Macroscale adhesion repeatability test result of a PBA DP-281 grafted mushroom-shaped micropillar array conducted at 10 mN preload and 10 μm/s retraction speed.

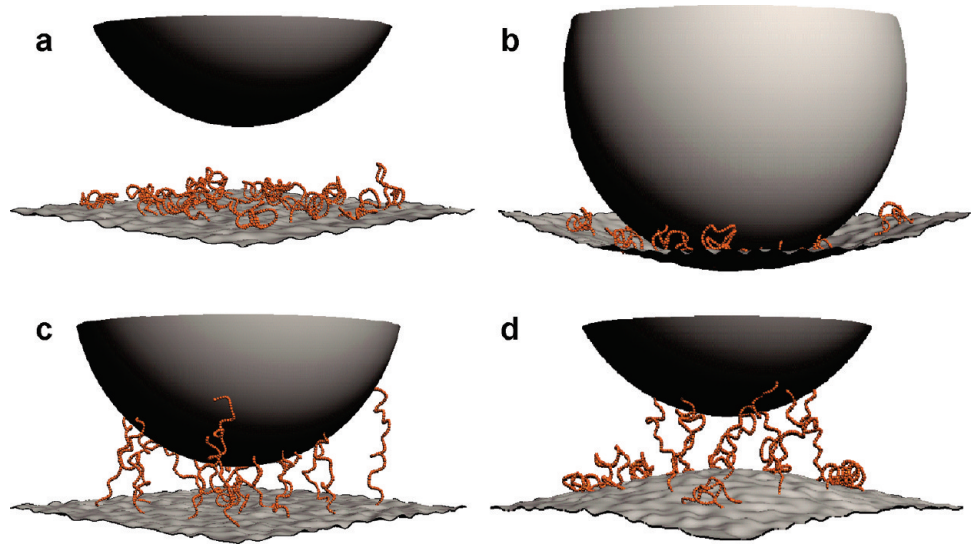

FIGURE 7. Schematic representation of the potential mechanism responsible for the increase of the adhesiveness of a flat elastomer surface in the presence of grafted polymer dangling chains (not to scale): (a) a spherical indenter approaches the dangling chains that are grafted onto the elastomer surface; (b) the indenter comes into contact with the chains and deforms the compliant backing layer; (c) when the sphere is withdrawn away from the surface, it stretches the polymer chains, which prolongs its contact with the surface and increases the amount of work necessary to perform before the surfaces are separated; (d) after becoming nearly fully stretched, the dangling chains pull the compliant backing layer, which further increases the work of adhesion.

compared to raw PDMS, which suggests additional enhancement mechanisms. This enhancement is hypothesized to arise from the energy dissipation due to the stretching of PBA chains on the surface (Figure 7), possibly in combination with bulk viscoelastic dissipation. Although raw PDMS is nearly elastic, especially at slow speeds, the subsurface grafting of hetero chains could cause a viscoelastic response of the material.

CONCLUSIONS

We have demonstrated the viability of a biologically inspired molecular and multilength scale structuring approach for tailoring the repeatable and enhanced adhesiveness of dangling chain elastomer surfaces. Through the generalization of the described fabrication process, other dangling hetero chains could be incorporated into elastomers and combined with micro-/nanoscale fiber fabrication methods to yield hierarchical fibrillar adhesives tailored for specific applications. One can envision that this new class of bioinspired repeatable adhesives will find a wide range of uses, such as attachment materials for climbing and biomedical robots, enhanced gripping gloves and shoes, and reusable adhesives in textile, space, packaging, medicine, and product design applications.

EXPERIMENTAL SECTION

Methods and Materials. All chemicals were purchased from Aldrich and Acros and used as received unless otherwise stated. Anisole and *n*-butyl acrylate (BA) were purchased from Acros and distilled under vacuum prior to use. PDMS (Sylgard 184), which comes in two parts, a base and a curing agent, was purchased from Dow Corning. CuBr, allyl 2-bromoisobutyrate (98%) and *N*,*N*,*N*′,*N*″,*N*″-pentamethyldiethylenetriamine (PMDETA) were purchased from Aldrich Chemical Co.

Scheme 1. Preparation of a PDMS Network Functionalized with ATRP Initiators Followed by Synthesis of PBA Chains from the Functionalized PDMS

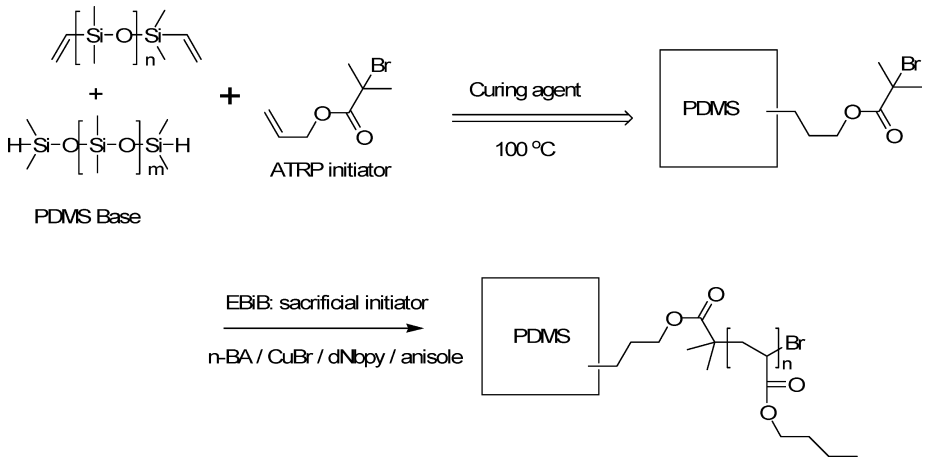

The apparent molecular weight and molecular weight distributions of PBA were measured on a GPC system consisting of a Waters 510 HPLC pump, three Waters UltraStyragel columns (100, 10^3, and 10^5 Å), and a Waters 410 differential refractive index detector, with a tetrahydrofuran (THF) flow rate of 1.0 mL/min; polystyrene was used as a calibration standard employing WinGPC software from Polymer Standards Service.

Synthesis. ***Flat PDMS Substrate Functionalized with ATRP Initiators.*** A 13.2 g portion of PDMS base, 1.7 g of curing agent, and 0.08 g of allyl 2-bromoisobutyrate were added to a Petri dish and degassed by vacuum for 25 min. The mixture was cured at 100 °C for 12 h to give a thin film (2 mm) of PDMS network. The cured PDMS film was cut into small pieces for further use.

PBA Chains from the Functionalized PDMS and a Silicon Wafer. In the ATRP grafting from flat surfaces, it has been reported that addition of the sacrificial initiators into the polymerization mixture was required for better control of polymerization (34, 35). This grafting from approach was applied to the synthesis of a network with dangling chains. The free (untethered) chains were generated from the sacrificial initiators. Some of these chains were terminated by radical coupling in solution, thereby spontaneously forming a sufficient amount of the deactivator.

The synthetic route for the PBA chains grafted from the PDMS substrate is outlined in Scheme 1. The curing process involves a platinum-catalyzed hydrosilylation reaction between vinyl groups from the siloxane base oligomers and hydrosilyl groups from the cross-linking oligomers, forming Si—CH_2CH_2—Si bonds. The —C═C— double bond from allyl 2-bromoisobutyrate added to the system also reacted with Si—H moieties, forming a PDMS network with covalently attached ATRP initiating moieties. The ATRP initiating groups should be present both inside of the PDMS network and on the surface. As the ratio of allyl 2-bromoisobutyrate to PDMS base was increased, incorporation of ATRP initiating groups was enhanced, resulting in a less cross-linked and mechanically softer PDMS network. PBA chains with several degrees of polymerization (DP) were grafted from PDMS networks (Table 1). CuBr/PMDETA was used as a catalyst system for polymerization of BA. Ethyl 2-bromoisobutyrate (EBiB) was used as the sacrificial initiator. The conversion of BA was determined by gas chromatography. The molecular weight and molecular weight distribution were obtained by GPC using polystyrene standards and THF as eluent (Figure 8). PBA chains were also grafted from the silicon surface for comparison by using the same conditions, which were used for grafting from the PDMS surface. The PBA film thickness was measured by ellipsometry for silicon-*g*-PBA samples, but it was not possible to measure the PBA film thickness on the surface of PDMS, due to a sparse dangling chain structure.

The general synthetic procedure for PBA chains grafted from the functionalized PDMS is described below (32). In a 50 mL Schlenk flask, a piece of PDMS film, BA (25.6 g, 200 mmol), ethyl 2-bromoisobutyrate (EBiB) (74 μL, 0.5 mmol), anisole (3 mL), and PMDETA (51 μL, 0.5 mmol) were added, and the reaction mixture was degassed by three freeze—pump—thaw

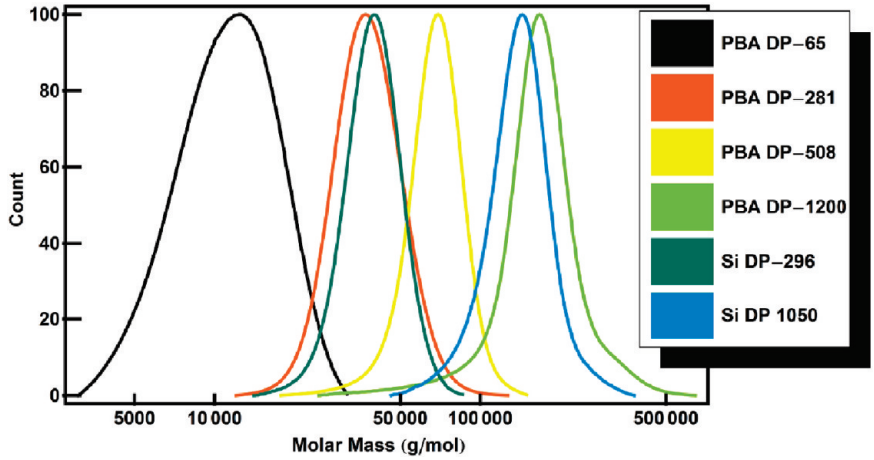

FIGURE 8. Gel permeation chromatography (GPC) traces of free PBA polymers initiated by the sacrificial initiator, EBiB.

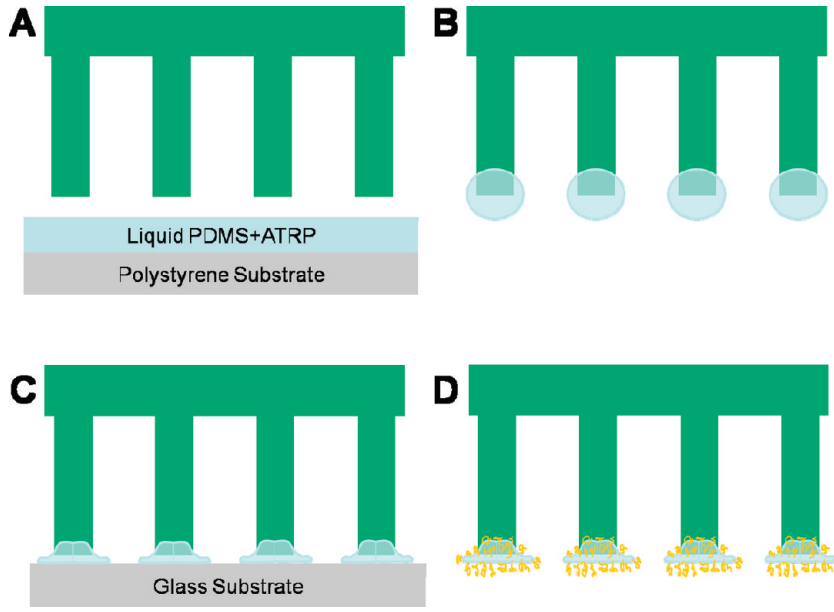

FIGURE 9. (A) PDMS with ATRP initiator is spun on a polystyrene surface for 1 min at 6000 rpm. (B) PDMS micropillars are dipped into the thin layer of PDMS with ATRP initiator to retrieve some PDMS with ATRP initiator on the tip of the pillars. (C) PDMS pillars are placed onto a glass substrate. (D) Upon curing, pillars are peeled off from the glass substrate and PBA molecular chains are grafted on the pillar tips using the ATRP process.

cycles. After the mixture was stirred for 0.5 h at room temperature, CuBr (0.072 g, 0.5 mmol) was added under nitrogen, and the flask was placed in a preheated oil bath at 70 °C. The polymerization was stopped after 7 h by cooling to room temperature and opening the flask to air. The PDMS piece which has PBA chains grafted in and from its surface was taken from the reaction mixture and soaked in THF for 12 h to remove free polymers, which could be adsorbed on the surface. This soaking process was repeated three times. The resulting product (PBA DP-281) was dried at room temperature for 24 h. For the synthesis of PBA chains from a silicon wafer, the same conditions were used, except an ATRP initiator modified silicon wafer was used instead of PDMS (33).

PBA Chains Grafted from the Tip Endings of Mushroom-Shaped PDMS Micropillars. A previously developed dip transfer method (11, 36−38) was adapted to fabricate elastomer mushroom-shaped micropillars (Figure 9). First, PDMS micropillars were created by molding a soft polyurethane (ST-1060, BJB Enterprises) negative template, which was generated by molding an array of SU-8 photoresist (SU-8 2025, MicroChem) pillars fabricated via ultraviolet light lithography. To form the mushroom shape, a thin layer of a PDMS mixture with ATRP initiator was spun onto a polystyrene substrate. PDMS micropillars were dipped into this thin layer to pick up some liquid PDMS with the ATRP initiator on their tips and then pressed to a glass surface. Upon curing, pillars were peeled off from the nonstick surface to form the spatula tips. Then, PBA molecular chains were grafted from the tip endings using the ATRP process. The backing layer thickness of the micropillars was 1.2 mm.

Carbon and Silicon Analysis. Carbon and silicon percentages were determined a Philips/FEI XL-30 field emission microscope equipped with an energy dispersive X-ray detector. Cross sections of the samples were cut with a razor blade and coated with ~1 nm thick platinum. The samples were placed in the SEM-EDX chamber, and several points along the cross-section of the samples (25 for PDMS-g-PBA, and 3 for PDMS with initiator and raw PDMS) were analyzed with an acquisition time of 30 s at 10 kV.

Nanoscale Characterization. AFM-based nanoscale adhesion measurements were performed with a Digital Instruments Nanoscope III MultiMode scanning probe microscope (Santa Barbara, CA) using a silicon cantilever probe. First, the photodiode sensitivity of the AFM system was calibrated. Then, the spring constant of the cantilever was calibrated using the thermal noise method (Thermal Tune option in Veeco's Nanoscope software (v 7.30)). This method measures the Brownian motion of the cantilever and converts the time domain measurement to the frequency domain. The spectrum is fit to a Lorentzian around the resonance frequency, and the software estimates the spring constant. Using this method, the probe stiffness used in the experiments was found to be 41 N/m. Due to the natural oxide layer on the probe under ambient conditions, the AFM probe tip material is taken as silicon dioxide. Force−volume images were acquired with a vertical engage J-scanner. AFM images were taken in the tapping mode with the same instrument using a silicon cantilever probe with a nominal spring constant of 40 N/m.

An analysis of the AFM images was carried out with the aid of custom code written in MATLAB 7.0 (MathWorks Inc., Natick, MA). To determine the pull-off force and dependence of pull-off force on probe retraction speed, each force curve in the force−volume image was averaged to find the average force curve. The pull-off force, F, was determined by using Hooke's law $F = k\,x$, where x is the maximum negative deflection and k is the spring constant of the cantilever. The maximum attractive force corresponds to the adhesion, and the area between the approach and retract curves reflects the overall work of adhesion.

To obtain the distributions of pull-out lengths and of the apparent Young modulus of the samples, each individual force curve in the force−volume image was used. The pull-out length was determined as the length required for the piezo stage to travel for the deflection to go from its minimum to the zero deflection on the retract portion of the force curve. The apparent Young modulus κ of the sample was determined by applying the Hertz contact mechanics model for a spherical indenter, where d, the distance indented, is proportional to the applied force, $F^{2/3}$. The proportionality constant, α, is defined as $\alpha = (3\pi/4R)^{1/3}\kappa^{2/3}$, where R is the radius of the indenter and $\kappa = ((1 - \nu_1^2)/E_1) + (1 - \nu_2^2)/E_2)^{-1}$ with ν_1 and ν_2 as the Poisson ratio of the indenter and sample, respectively, and E_1 and E_2 as the Young modulus of the indenter and sample, respectively, assuming constant material properties. When the indenter is

much harder than the sample, i.e. $E_1 \gg E_2$, the first term in κ can be ignored. The equation $d = \alpha F^{2/3}$ can be fit to the data, where d is the deflection from the onset of contact to minus the distance the piezo travels on the approach portion of the force curve, and F, the applied force, is the deflection times the spring constant of the cantilever. The apparent Young modulus of the sample was calculated from this equation assuming an AFM probe tip radius of 10 nm and a sample Poisson ratio of 0.5. It should be noted that due to the uncertainties of the indenter geometry and complex nature of PBA grafted PDMS, this type of analysis represents considerable oversimplification, and its results cannot be treated as a rigorous measurement of the Young modulus of the sample. The obtained value, henceforth referred to as an apparent Young modulus, provides nevertheless useful means for ascertaining the overall impact of PBA on the local effective stiffness of studied materials.

Macroscale Adhesion Characterization. For performing macroscale adhesion measurements, a custom tensile force measurement system was set up using an automated stage (MFA-CC; Newport), a 50 g load cell (GSO-50; Transducer Techniques Inc.), and a 6 mm diameter glass hemisphere (QU-HS-12; ISP Optics). The glass hemisphere was attached to the glass slide on the load cell using superglue (Loctite 404), whereas the PDMS sample was affixed to the glass slide on the automated stage using double-sided tape. The glass hemisphere was moved toward the PDMS sample at a preset constant velocity until the glass contacted the PDMS sample. After the contact was achieved and a preset preload was reached, the glass hemisphere was retracted from the sample with a constant speed. The adhesion force is the maximum measured force while the sample was being pulled away from the surface. During the measurement, the output voltage was continuously fed into a data acquisition board and the computer software read the voltage, calculated the force on the load cell, and gave output commands to move the stage accordingly. A hemisphere glass piece was chosen over a flat glass piece as the adhering surface to eliminate measurement errors due to misalignment. Furthermore, using a hemispherical probe for testing is appropriate for the comparing the adhesion measurements to AFM experiments and the smooth sphere indenter contact represents a single asperity surface roughness, enabling us to characterize the rough surface adaptation and adhesion for the fibrillar structures. Force–distance plots for flat and fibrillar PDMS surfaces with and without PBA chains for 6 mN preload at 1 μm/s speed are displayed in Figure 2 in the Supporting Information as sample data. Sawtooth-shaped behavior during detachment in fibrillar samples corresponds to discrete detachment of pillars gradually. Each step shows the adhesion of single or several pillars.

The same measurement system was used to measure the Young modulus and the thermodynamic work of adhesion for the flat nonpatterned PDMS substrates. The contact radius is tracked and measured by a camera attached to the inverted microscope and is synchronized with the force data. The force data are obtained at 1 μm/s indenter speed. Figure 10 shows the load-deformation plots obtained for raw flat PDMS and PBA DP-281 samples. For a typical Johnson–Kendall–Roberts experiment, under equilibrium conditions, the load and the deformation are related as (39)

$$\frac{a^{1.5}}{R} = \frac{3}{4\kappa}\frac{P}{a^{1.5}} + \left(\frac{9\pi w}{2\kappa}\right)^{0.5} \qquad (1)$$

where a is the contact radius, P is the load, R is the radius of the hemispherical indenter, and κ is the apparent Young modulus. On the basis of the assumption that the thermodynamic work of adhesion (w) is approximately equal to the energy release rate (G) during crack closing, κ can be calculated from the slope of the crack advancement (loading) portion of the load-deformation plot (Figure 10) using eq 1. w can be found by plugging in κ in eq 1, where the Poisson ratio is assumed to be 0.5 and $R = 3$ mm.

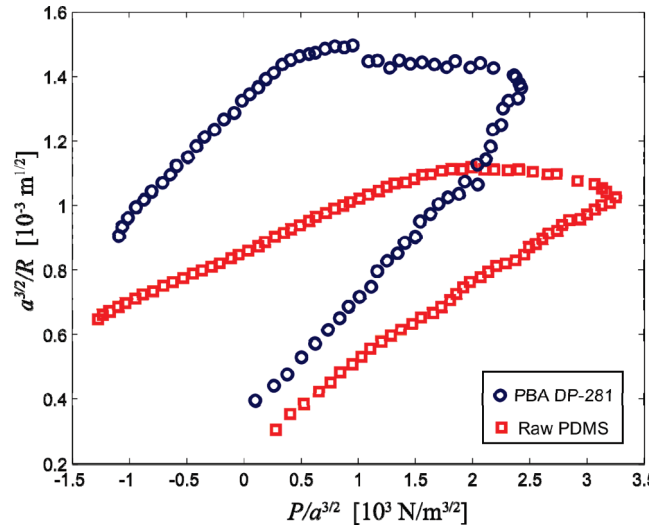

FIGURE 10. Experimental load-deformation plots for raw PDMS and PBA DP-281 samples.

Supporting Information Available: Three figures giving sample AFM force–distance curves of PBA chains grafted from flat PDMS, adhesion data of PBA chains grafted from silicon substrates, and sample force–distance plots for flat and fibrillar PDMS surfaces with and without grafted PBA chains. This material is available free of charge via the Internet at http://pubs.acs.org.

REFERENCES AND NOTES

(1) Autumn, K.; Liang, Y. A.; Hsleh, S. T.; Zesch, W.; Chan, W. P.; Kenny, T. W.; Fearilng, R.; Full, R. J. *Nature (London)* **2000**, *405*, 681–686.
(2) Autumn, K.; Sitti, M.; Liang, Y. A.; Peattie, A. M.; Hansen, W. R.; Sponberg, S.; Kenny, T. W.; Fearing, R.; Israelachvili, J. N.; Full, R. J. *Proc. Natl. Acad. Sci. U.S.A.* **2002**, *99*, 12252–12256.
(3) Arzt, E.; Gorb, S.; Spolenak, R. *Proc. Natl. Acad. Sci. U.S.A.* **2003**, *100*, 10603–10606.
(4) Persson, B. N. J. *J. Chem. Phys.* **2003**, *118*, 7614–7621.
(5) Gao, H.; Yao, H. *Proc. Natl. Acad. Sci. U.S.A.* **2004**, *101*, 7851–7856.
(6) Gorb, S.; Varenberg, M.; Peressadko, A.; Tuma, J. *J. R. Soc. Interface* **2007**, *4*, 271–275.
(7) Kim, S.; Sitti, M. *Appl. Phys. Lett.* **2006**, *89*, 261911/1–261911/3.
(8) Kim, S.; Sitti, M.; Hui, C.-Y.; Long, R.; Jagota, A. *Appl. Phys. Lett.* **2007**, *91*, 161905/1–161905/3.
(9) Aksak, B.; Murphy, M. P.; Sitti, M. *Langmuir* **2007**, *23*, 3322–3332.
(10) Crosby, A. J.; Hageman, M.; Duncan, A. *Langmuir* **2005**, *21*, 11738–11743.
(11) del Campo, A.; Greiner, C.; Alvarez, I.; Arzt, E. *Adv. Mater. (Weinheim, Ger.)* **2007**, *19*, 1973–1977.
(12) Glassmaker, N. J.; Jagota, A.; Hui, C.-Y.; Noderer, W. L.; Chaudhury, M. K. *Proc. Natl. Acad. Sci. U.S.A.* **2007**, *104*, 10786–10791.
(13) Lee, H.; Lee, B. P.; Messersmith, P. B. *Nature* **2007**, *448*, 338–341.
(14) Sitti, M.; Fearing, R. S. *J. Adhes. Sci. Technol.* **2003**, *17*, 1055–1073.
(15) Geim, A. K.; Dubonos, S. V.; Grigorieva, I. V.; Novoselov, K. S.; Zhukov, A. A.; Shapoval, S. Y. *Nat. Mater.* **2003**, *2*, 461–463.
(16) Majidi, C.; Groff, R. E.; Maeno, Y.; Schubert, B.; Baek, S.; Bush, B.; Maboudian, R.; Gravish, N.; Wilkinson, M.; Autumn, K.; Fearing, R. S. *Phys. Rev. Lett.* **2006**, *97*, 076103/1–076103/4.
(17) Northen, M. T.; Turner, K. L. *Nanotechnology* **2005**, *16*, 1159–1166.
(18) Aksak, B.; Sitti, M.; Cassell, A.; Li, J.; Meyyappan, M.; Callen, P. *Appl. Phys. Lett.* **2007**, *91*, 061906/1–061906/3.

(19) Ge, L.; Sethi, S.; Ci, L.; Ajayan, P. M.; Dhinojwala, A. *Proc. Natl. Acad. Sci. U.S.A.* **2007**, *104*, 10792–10795.
(20) Qu, L.; Dai, L. *Adv. Mater. (Weinheim, Ger.)* **2007**, *19*, 3844–3849.
(21) Zhao, Y.; Tong, T.; Delzeit, L.; Kashani, A.; Meyyappan, M.; Majumdar, A. *J. Vac. Sci. Technol., B: Microelectron. Nanometer Struct. Process., Meas., Phenom.* **2006**, *24*, 331–335.
(22) Hui, C. Y.; Glassmaker, N. J.; Tang, T.; Jagota, A. *J. R. Soc. Interface* **2004**, *1*, 35–48.
(23) Majumder, A.; Ghatak, A.; Sharma, A. *Science (Washington, D.C.)* **2007**, *318*, 258–261.
(24) She, H.; Malotky, D.; Chaudhury, M. K. *Langmuir* **1998**, *14*, 3090–3100.
(25) Patten, T. E.; Xia, J.; Abernathy, T.; Matyjaszewski, K. *Science (Washington, D.C.)* **1996**, *272*, 866–868.
(26) Ahn, D.; Shull, K. R. *Macromolecules* **1996**, *29*, 4381–4390.
(27) Wu, Y.; Huang, Y.; Ma, H. *J. Am. Chem. Soc.* **2007**, *129*, 7226–7227.
(28) Bistac, S.; Galliano, A.; Schmitt, M. *J. Phys.: Condens. Matter* **2008**, *20*, 354015/1–354015/6.
(29) Bizet, S.; Galy, J.; Gerard, J.-F. *Macromolecules* **2006**, *39*, 2574–2583.
(30) Budinski-Simendic, J.; Spirkova, M.; Dusek, K.; Dikic, T.; Randicevic, R.; Prendzov, S.; Krakovsky, I.; Ilavsky, M. *Mater. Sci. Forum* **2006**, *518*, 399–404.
(31) Vaenkatesan, V.; Li, Z.; Vellinga, W.-P.; de Jeu, W. H. *Polymer* **2006**, *47*, 8317–8325.
(32) Matyjaszewski, K.; Dong, H.; Jakubowski, W.; Pietrasik, J.; Kusumo, A. *Langmuir* **2007**, *23*, 4528–4531.
(33) Matyjaszewski, K.; Miller, P. J.; Shukla, N.; Immaraporn, B.; Gelman, A.; Luokala, B. B.; Siclovan, T. M.; Kickelbick, G.; Vallant, T.; Hoffmann, H.; Pakula, T. *Macromolecules* **1999**, *32*, 8716–8724.
(34) Ejaz, M.; Yamamoto, S.; Ohno, K.; Tsujii, Y.; Fukuda, T. *Macromolecules* **1998**, *31*, 5934–5936.
(35) Jeyaprakash, J. D.; Samuel, S.; Dhamodharan, R.; Ruhe, J. *Macromol. Rapid Commun.* **2002**, *23*, 277–281.
(36) Murphy, M. P.; Aksak, B.; Sitti, M. *J. Adhes. Sci. Technol.* **2007**, *21*, 1281–1296.
(37) Murphy, M. P.; Aksak, B.; Sitti, M. *Small* **2009**, *5*, 170–175.
(38) Murphy, M. P.; Kim, S.; Sitti, M. *ACS Appl. Mater. Interfaces* **2009**, *1*, 849–855.
(39) Chaudhury, M. K. *Mater. Sci. Eng., R* **1996**, *R16*, 97–159.

AM9004368